JOURNAL OF GUIDANCE, CONTROL, AND DYNAMICS
Vol. 27, No. 3, May–June 2004

Aircraft Autopilot Analysis and Envelope Protection for Operation Under Icing Conditions

Vikrant Sharma,* Petros G. Voulgaris,† and Emilio Frazzoli‡
University of Illinois at Urbana–Champaign, Urbana, Illinois 61801-2935

The behavior of a typical autopilot structure is studied for flight under icing conditions. The study is based on a Twin Otter aircraft model and focuses on the pitch attitude behavior. A quadratic stability analysis using linear matrix inequalities is conducted to show that the time-varying closed-loop system maintains quadratic stability under icing conditions. In addition, the problem of envelope protection in the presence of icing is considered; in particular, how to maintain the angle-of-attack within the stall limits which are time varying. Based on steady-state behavior, a practical envelope protection scheme is developed and tested via simulation.

I. Introduction

AIRCRAFT accidents continue to occur due to the formation of ice on aircraft in flight. The development of safer, more reliable and affordable aircraft must include better solutions for flight in icing and bad weather conditions. The primary cause of these accidents is the effect of ice accretion on the performance, stability, and control of the aircraft.[1] Accidents occur when aircraft are not properly protected against ice accretion either on the ground or in flight. As mentioned in Ref. 1, this situation may result from an inadequate ice protection system or aircraft operation outside of the iced aircraft flight envelope. Icing accidents can be prevented in two ways: 1) icing conditions can be avoided, and 2) the aircraft system can be designed and operated in an ice-tolerant manner. For all aircraft, ice avoidance is the desired goal for increased safety. However, for commercial aircraft, where revenues and schedules must be maintained, ice tolerance will continue to be the preferred method for all but the most severe icing conditions. Currently a project on developing smart icing systems (SIS) to deal with this problem of icing is being carried out by a group of researchers at the University of Illinois.[2] The goal of the SIS research is to improve the safety of operations in icing conditions. This paper is a result of this SIS research. It studies the effects of ice accretion on the autopilot stability and performance and also develops techniques for envelope protection (EP) with the autopilot in operation under icing conditions. Current practice recommendations dictate that the autopilot system be shut down immediately when ice accretion is reported during the flight. The research reported here aims at taking a step in the direction of developing an autopilot system that is reliable and robust to icing conditions. This autopilot system will be tested by integrating it into a high-fidelity real-time simulator platform, the Icing Encounter Flight Simulator (IEFS),[3] currently being developed at the University of Illinois.

Section II presents the longitudinal pitch attitude hold (PAH) mode of the autopilot and describes its structure and the closed-loop state-space form used for analysis in subsequent sections. Section III analyzes the stability of the PAH autopilot under icing conditions. Section IV is devoted to the development of a practical EP module for the PAH autopilot. Finally, Sec. V concludes the paper with remarks on the research presented and future directions.

II. Autopilot Model

The research reported in this paper was conducted for the PAH mode of the aircraft autopilot because it is at the heart of the longitudinal control system of the aircraft. The function of this mode, as the name suggests, is to track the pitch angle commands issued by the pilot. The controller structure used for this purpose[4] is a proportional integral derivative (PID) controller. This autopilot structure was selected for the Twin Otter because it represents a standard configuration for autopilot systems. The PAH mode controls the pitch angle by applying appropriate deflections of the elevator if the actual pitch angle differs from the desired reference value. The structure of the PAH mode with the PID controller is shown in Fig. 1. The desired reference value of the pitch angle to be tracked is denoted by θ_{ref} and can be dynamic in nature. The pitch angle of the aircraft is fed back to ensure that the desired pitch angle is attained. A proportional and integral controller is applied to make sure that no steady-state errors in the pitch angle will remain. A feedback loop of the pitch rate (q) to the elevator has been included to compensate for the small decrease in damping of the short period mode due to feedback. In Fig. 1, the "A/C dynamics" block contains the aircraft's dynamical equations. (See Ref. 5 for a description of how these equations are implemented in the flight dynamics code and the Twin Otter aircraft parameters.) The actuator dynamics block contains a third-order dynamic model of the actuators and cables to the control surfaces as used in Ref. 4. The gains used by the controller, denoted by k_i, k_θ, and k_q, are scheduled in terms of the aircraft velocity obtained at different trim velocities under clean conditions. Table 1 shows the values for these gains at different flying velocities.

These gain values were chosen to have good gain and phase margins at all operating conditions. Table 2 shows the gain and phase margin values of the closed loop broken at the control input. Besides the PAH autopilot there are other modes including the altitude hold, heading hold, and roll attitude hold that use similar classical control structures as the one described here for the PAH autopilot. For details of these structures we refer to Ref. 4. The altitude hold mode is used to maintain a reference altitude, which is specified by the pilot. This mode uses the PAH mode as an inner loop, indicating that the PAH mode forms the basic structure for the longitudinal autopilot modes, hence justifying the importance of analyzing it.[4]

For all these modes the gains were chosen to provide good performance and robustness characteristics comparable to the PAH autopilot. A sample of responses is provided in Figs. 2a, 2b, and 2c. The atmospheric disturbances and sensor noise were incorporated into all these models. The external disturbances are mainly due to nonsteady

Received 14 March 2003; revision received 5 July 2003; accepted for publication 8 July 2003.

*Graduate Student, Department of Aeronautical and Astronautical Engineering and the Coordinated Science Laboratory, 1308 W. Main Street; vsharma@uiuc.edu.

†Associate Professor, Department of Aeronautical and Astronautical Engineering and the Coordinated Science Laboratory, 1308 W. Main Street; petros@control.csl.uiuc.edu. Member AIAA.

‡Assistant Professor, Department of Aeronautical and Astronautical Engineering and the Coordinated Science Laboratory, 1308 W. Main Street; frazzoli@uiuc.edu. Member AIAA.

atmosphere and sometimes due to ground effect. The wind profile, which simulates the earth boundary-layer effects, was based on the International Civil Aviation Organization (ICAO) standard atmosphere. Stochastic disturbances were used as means to describe atmospheric disturbances. The Dryden spectral density functions were used to fit the theoretical and experimental data on atmospheric turbulence. The atmospheric turbulence was modeled as white noise passing through a linear filter. (For more details on the parameters involved and their values, the reader is referred to Ref. 5.) The sensor noise was incorporated to represent the uncertainties resulting due to measurements obtained from various devices. Band-limited white Gaussian generators were used to represent the noise, and the amplitudes used were based on sensor uncertainties given by Ratvasky and Ranaudo.[6] The actual amplitudes used were twice those given by Ratvasky and Ranaudo.[5] The PAH autopilot model described in this section has already been incorporated into the IEFS.[7]

A. Iced Aircraft Model

This section describes how the aircraft dynamics are affected by icing. Because the study in this paper is limited to the longitudinal motion of the aircraft, only the linearized longitudinal flight dynamics of the aircraft are considered, as follows[8]:

$$\dot{u} = -g\theta\cos(\Theta_0) + \left(X_u + X_{T_u}\right)u + X_\alpha\alpha + X_{\delta_e}\delta_e \quad (1)$$

$$\dot{w} = -g\theta\sin(\Theta_0) + Z_u u + Z_\alpha\alpha + Z_{\dot{\alpha}}\dot{\alpha} + Z_{\delta_e}\delta_e + (Z_q + U_0)q \quad (2)$$

$$\dot{q} = \left(M_u + M_{T_u}\right)u + \left(M_\alpha + M_{T_\alpha}\right)\alpha + M_{\dot{\alpha}}\dot{\alpha} + M_q q + M_{\delta_e}\delta_e \quad (3)$$

where u is the forward velocity; w is the downward velocity; q is the pitch rate; θ is the pitch angle; α is the angle-of-attack; and δ_e is the elevator deflection angle; U_0 and Θ_0 represent the trim values of forward velocity and pitch angle, respectively; and M_*, Z_*, and X_* are the stability and control derivatives as appropriate. The effects of icing are manifested in these stability and control derivatives. During an icing encounter, the stability and control derivatives will change slowly over a period of several minutes. It was reported in Ref. 6 that the only significant changes occur in the M_α, M_q, Z_α, Z_q, X_α, and $(X_u + X_{T_u})$ stability derivatives and in the M_{δ_e} and Z_{δ_e} control derivatives. Values of these parameters for the Twin Otter for both the clean and the iced case can be viewed in the literature.[9] Flight tests have been conducted and reported[10] that provide data on the changes in these parameters.

These changes due to icing can be captured through an icing severity parameter. In particular, a linear variation of the parameters with respect to this icing severity factor was used as reported in Ref. 1:

$$C_{(A)\text{iced}} = \left(1 + \eta K_{C_{(A)}}\right)C_{(A)} \quad (4)$$

In this equation, η is the so-called aircraft icing parameter. It is a time-varying parameter that represents the amount and severity of the icing encounter at the given flying conditions for a particular aircraft for operation in the linear aerodynamic regime. For details on the variation of aircraft parameters in the nonlinear aerodynamic regime, the reader is referred to Ref. 11. The term $K_{C_{(A)}}$ represents the change in an aircraft parameter $C_{(A)}$ that is constant for a given aircraft. $C_{(A)}$ is any arbitrary performance, stability, or control derivative that is affected by ice accretion, and $C_{(A)\text{iced}}$ is its value under icing. For the linearized stability analysis conducted in the next section, it will be assumed that, at a given condition, the maximum possible value of the icing parameter η, denoted by $\eta_{\max}$, is known and, hence, η can attain values between 0 and $\eta_{\max}$ at that condition. In other words, η is a time-varying parameter that increases from $\eta = 0$ when the aircraft is clean, to a fully iced value of $\eta_{\max}$. A typical value of $\eta_{\max}$ is 0.1.

The nonlinear PAH closed-loop system under icing conditions can be linearized and a state-space system is obtained in the next subsection.

Table 1 Gains for the PAH autopilot at different velocities

Velocity, m/s	k_θ	k_i	k_q
40	−1.1	0.5	−0.1931
50	−1.014	0.5	−0.1431
60	−0.9	0.5	−0.0631
70	−1.016	0.5	−0.2631

Table 2 Gain and phase margins for the PAH autopilot at different velocities

Velocity, m/s	Gain margin, db	w_{GM}, rad/s	Phase margin, deg	w_{PM}, rad/s
40	12.49	19.782	105.98	3.1388
50	20.228	18.029	75.287	2.1388
60	16.196	18.658	81.96	2.4864
70	10.425	19.812	94.833	4.0177

B. Closed-Loop State-Space System

To conduct a quadratic stability analysis of the Twin Otter longitudinal behavior under icing conditions, the nonlinear aircraft model is linearized about various trim points. The original aircraft linearized system has 12 states, defined by

$$x_{\text{aircraft}} = [V \quad \alpha \quad \beta \quad p \quad q \quad r \quad \phi \quad \theta \quad \psi \quad x_e \quad y_e \quad H]^T \quad (5)$$

where $V, \alpha, \beta, p, q, r, \phi, \theta, \psi, x_e, y_e$, and H are the aircraft's velocity, angle-of-attack, sideslip angle, roll angle, pitch rate, yaw rate, yaw angle, pitch angle, roll angle, X coordinate in earth fixed reference frame, Y coordinate in earth fixed reference frame, and altitude above sea level, respectively. Now, because the aircraft longitudinal

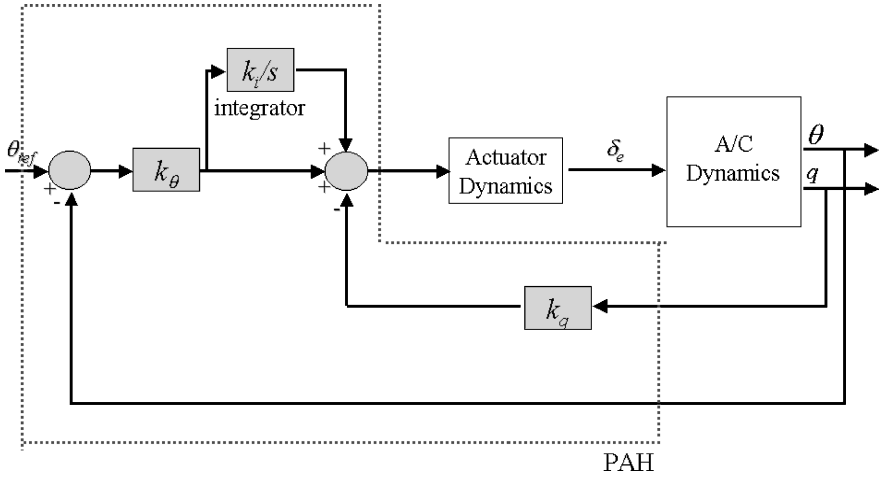

Fig. 1 The block diagram of the closed-loop PAH autopilot model.

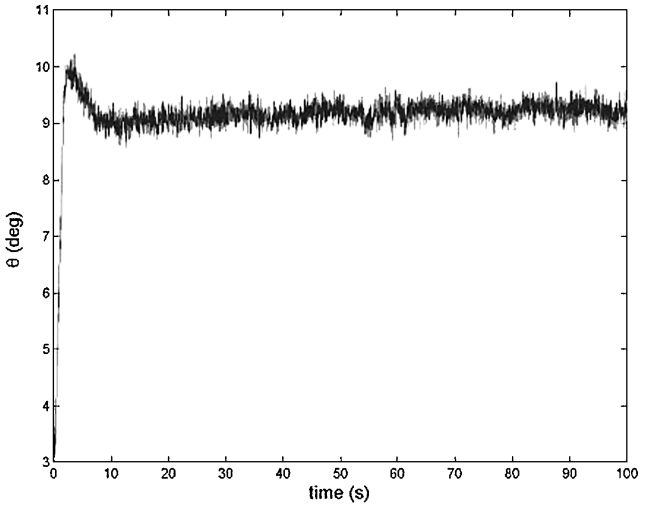

a)

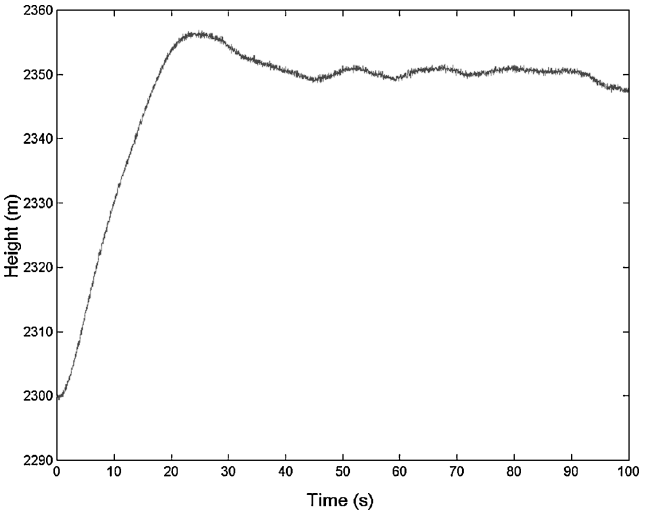

b)

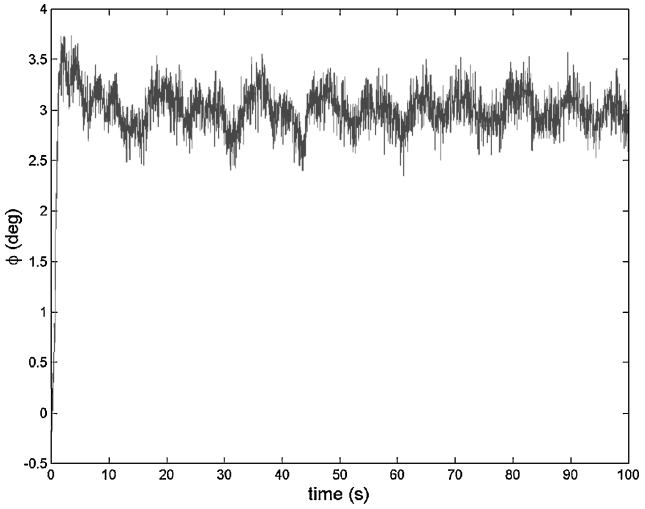

c)

Fig. 2 Responses of different autopilot modes: a) pitch tracking by the PAH autopilot to a pitch up input of 6 deg at 60 m/s, b) altitude response of altitude hold autopilot to the reference altitude command of 50 m at a height of 2300 m, and c) roll-angle tracking of the roll attitude hold autopilot to a roll command of 3 deg.

and lateral dynamics can be decoupled and have very little effect on each other, the full linearized aircraft model can be reduced to a model with four longitudinal states for PAH autopilot design and analysis.[12] The states chosen are

$$x_1 = [V \quad \alpha \quad q \quad \theta]^T \tag{6}$$

For the Twin Otter aircraft parameters, the reader is referred to Ref. 5. Due to the affine dependence of the aircraft parameters on the icing parameter η as demonstrated by Eq. (4), the linearized state-space system matrices of the original nonlinear aircraft model are found to be affinely dependent on the icing parameter; that is, the linearized aircraft open-loop state-space model can be written as a time-varying system of the form

$$\dot{x}_1 = A_{\text{ac}} x_1 + B_{\text{ac}} u_1 \tag{7}$$

where

$$A_{\text{ac}} = A_0 + \eta(t) A_1, \qquad B_{\text{ac}} = B_0 + \eta(t) B_1 \tag{8}$$

u_1 is the elevator deflection, and x_1 is given by Eq. (6). A_0 and B_0 represent the aircraft state-space system matrices for clean conditions, A_1 and B_1 can be viewed as the matrices representing the change in the dynamics due to the presence of ice, and $\eta(t)$ is the time-varying icing parameter. To obtain the state-space system for the closed-loop PAH model shown in Fig. 1, the gains and the reference signals are defined in a vector form for convenience of analysis as follows:

$$x_{\text{ref}} = [0 \quad 0 \quad 0 \quad \theta_{\text{ref}}]^T, \qquad K_\theta = [0 \quad 0 \quad 0 \quad k_\theta]$$
$$K_q = [0 \quad 0 \quad k_q \quad 0], \qquad K_i = k_i \tag{9}$$

Let the actuator dynamics be given by

$$\dot{x}_3 = A_{\text{elv}} x_3 + B_{\text{elv}} u_3, \qquad u_1 = C_{\text{elv}} x_3 + D_{\text{elv}} u_3 \tag{10}$$

The input to the actuator dynamics denoted by u_3 is given by

$$u_3 = -K_\theta (x_1 - x_{\text{ref}}) + x_2 - K_q x_1 \tag{11}$$

where x_2 is the state added to the system due to the integrator in the control loop and is given by

$$\dot{x}_2 = -K_\theta K_i (x_1 - x_{\text{ref}}) \tag{12}$$

The whole system with states x_1, x_2, and x_3 then can be represented by the following state-space equation:

$$\begin{bmatrix} \dot{x}_1 \\ \dot{x}_2 \\ \dot{x}_3 \end{bmatrix} = \begin{bmatrix} A_{\text{ac}} - B_{\text{ac}} D_{\text{elv}} (K_q + K_\theta) & B_{\text{ac}} D_{\text{elv}} & B_{\text{ac}} C_{\text{elv}} \\ -K_i K_\theta & 0 & 0 \\ -B_{\text{elv}} (K_q + K_\theta) & B_{\text{elv}} & A_{\text{elv}} \end{bmatrix} \begin{bmatrix} x_1 \\ x_2 \\ x_3 \end{bmatrix}$$
$$+ \begin{bmatrix} B_{\text{ac}} D_{\text{elv}} K_\theta \\ -K_i K_\theta \\ B_{\text{elv}} K_\theta \end{bmatrix} x_{\text{ref}} \tag{13}$$

where $x_1 \in \Re^4$, $x_2 \in \Re$, and $x_3 \in \Re^3$. The preceding system can be rewritten as

$$\dot{x} = A_{\text{closed}} x + B_{\text{closed}} x_{\text{ref}} \tag{14}$$

Now using Eq. (8), the closed-loop matrices of the preceding system can be rewritten in the following form and are seen to be affinely dependent on the icing parameter η:

$$A_{\text{closed}}(\eta) = \begin{bmatrix} A_0 - B_0 D_{\text{elv}} (K_q + K_\theta) & B_0 D_{\text{elv}} & B_0 C_{\text{elv}} \\ -K_i K_\theta & 0 & 0 \\ -B_{\text{elv}} (K_q + K_\theta) & B_{\text{elv}} & A_{\text{elv}} \end{bmatrix}$$

$$+\eta(t)\begin{bmatrix} A_1 - B_1 D_{\text{elv}}(K_q + K_\theta) & B_1 D_{\text{elv}} & B_1 C_{\text{elv}} \\ 0 & 0 & 0 \\ 0 & 0 & 0 \end{bmatrix} \tag{15}$$

$$B_{\text{closed}}(\eta) = \begin{bmatrix} B_0 D_{\text{elv}} K_\theta \\ -K_i K_\theta \\ B_{\text{elv}} K_\theta \end{bmatrix} + \eta(t)\begin{bmatrix} B_1 D_{\text{elv}} K_\theta \\ 0 \\ 0 \end{bmatrix} \tag{16}$$

III. Quadratic Stability

A. Definition and Problem Setup

We will consider the question of stability analysis of the system defined by system (14). The question is, with $\theta_{\text{ref}} = 0$, does system (14) satisfy $\lim_{t\to\infty} x(t) = 0$ for every initial condition $x(0)$ and $\eta \in [0, \eta_{\max}]$? If so, we say that the system is robustly stable over $\triangle = [0, \eta_{\max}]$. One class of sufficient conditions for robust stability is based on the notion of quadratic stability.

Definition 1: The system given by the equation:

$$\dot{x} = A_{\text{closed}}[\eta(t)]x \tag{17}$$

is said to be quadratically stable for all time varying perturbations $\eta(t)$ lying in the set $\triangle = [0, \eta_{\max}]$ if and only if there exists a single quadratic Lyapunov function $V(x) = x^T K x$, $K > 0$ whose derivative is negative along every trajectory of the system, i.e.

$$\frac{\mathrm{d}V[x(t)]}{\mathrm{d}t} = x^T\left\{A^T_{\text{closed}}[\eta(t)]K + K A_{\text{closed}}[\eta(t)]\right\}x < 0$$

for all $\eta(t) \in \triangle$, or equivalently, there exists $K = K^T > 0$ such that

$$A^T_{\text{closed}}[\eta(t)]K + K A_{\text{closed}}[\eta(t)] < 0 \tag{18}$$

for all $\eta(t) \in \triangle$.[§]

Note that, in general, quadratic stability of the system for an uncertainty class $\triangle$ places an infinite number of constraints on the symmetric matrix K. In this section, this problem of checking quadratic stability is converted into a numerically tractable one by using the way the uncertainty η enters the system. To analyze the quadratic stability of the PAH model, that is, for the case $\theta_{\text{ref}} = 0$, we use the fact that the closed-loop matrices are affinely dependent on η. This icing parameter is a function of time and is treated as a time-varying uncertainty parameter that varies in a known interval; that is, it is known that $\eta(t) \in [0, \eta_{\max}] = \triangle$, as indicated in the previous section. Given the fact that the closed-loop state-space matrix A_{closed} given by Eq. (15) is affinely dependent on the parameter η, the condition for the quadratic stability given by Eq. (18) of the system denoted by Eq. (17) can be simplified to checking the existence of a finite number of linear matrix inequalities (LMIs).[13,§] A few more definitions are useful in showing this:

Definition 2: The convex hull $co(\triangle_0)$ of a set $\triangle_0$ is the intersection of all convex sets containing $\triangle_0$.[§]

Proposition 1: Let $f : \triangle \to \Re$ be a convex function where $\triangle = co(\triangle_0)$. Then $f(x) \le \gamma$ for all $x \in \triangle$ if and only if $f(x) \le \gamma$ for all $x \in \triangle_0$.[§]

Defining $\triangle_0 = \{0, \eta_{\max}\}$, it is observed that $\triangle = co(\triangle_0)$. Now fix $y \in \Re^8$ and consider the mapping $f_y : \triangle \to \Re$ defined by

$$f_y(\eta) := y^T\left\{A^T_{\text{closed}}[\eta(t)]K + K A_{\text{closed}}[\eta(t)]\right\}y$$

The domain of this mapping is a convex set and by definition $\triangle = co(\triangle_0)$. Furthermore, because $A_{\text{closed}}(\eta)$ is an affine function of η it follows that $f_y(\eta)$ is a convex function of η. Now, Proposition 1 yields that $f_y(\eta) < 0$ for all $\eta \in \triangle$ if and only if $f_y(\eta) < 0$ for all $\eta \in \triangle_0$. Because y is arbitrary it follows that

$$A^T_{\text{closed}}[\eta(t)]K + K A_{\text{closed}}[\eta(t)] < 0, \eta(t) \in \triangle$$

[§]Taken from Scherer, C., and Weiland, S., "Linear Matrix Inequalities in Control," Course Notes from the Dutch Institute of Systems and Control.

Table 3 α values for the model linearized at different velocities for $\eta_{\max} = 0.1$

Velocity, m/s	α
60	−0.089
70	−0.1005
80	−0.1119

if and only if

$$A^T_{\text{closed}}(\eta)K + K A_{\text{closed}}(\eta) < 0, \eta \in \triangle_0$$

In other words we can say that system (14) is quadratically stable for all time-varying perturbations $\eta(t) \in \triangle$ if there exists a positive definite matrix K such that

$$A^T_{\text{closed}}(\eta = 0)K + K A_{\text{closed}}(\eta = 0) < 0$$

$$A^T_{\text{closed}}(\eta = \eta_{\max})K + K A_{\text{closed}}(\eta = \eta_{\max}) < 0 \tag{19}$$

B. Results

A stability analysis in terms of the decay rate of the system was conducted, using the result in Eq. (19) mentioned in the previous subsection, for various operational conditions for the linearized closed-loop model using the Linear Matrix Inequalities toolbox in MATLAB.[14] The idea was to look for the minimum value of the parameter $\alpha < 0$, also called the decay rate, for which $\dot{V}(x)/V(x) < \alpha$. This would mean that $V(t) \le e^{\alpha t}V(0)$ for all trajectories and, hence, shows that α is a measure of the rate at which the system response decays with time. The problem of finding the decay rate is equivalent to the problem of finding the minimum possible value of $\alpha < 0$, for which there exists a positive definite matrix K that satisfies

$$A^T_{\text{closed}}(\eta = 0)K + K A_{\text{closed}}(\eta = 0) < \alpha K$$

$$A^T_{\text{closed}}(\eta = \eta_{\max})K + K A_{\text{closed}}(\eta = \eta_{\max}) < \alpha K \tag{20}$$

The feasibility of the preceding two LMIs for some $K > 0$ guarantees the stability of the closed-loop system in Eq. (17) with $\eta(t) \in [0, \eta_{\max}]$. The MATLAB command "decay" looks for the minimum possible value of α for which Eq. (20) is feasible and, thus, gives the decay rate. The system was analyzed for decay rates at different velocities. Table 3 shows the decay rate α for aircraft models linearized at different trim velocities with $\eta_{\max} = 0.1$. The linear stability analysis of the PAH autopilot suggests that the autopilot will maintain longitudinal stability even in the presence of icing. Figures 3a, 3b, 3c, and 3d show the PAH autopilot angle of attack, pitch, elevator, and velocity responses, respectively, for an aircraft initially trimmed at $v = 60$ m/s at a height of 2300 m to a pitch-up maneuver of 5 deg. Ice builds up linearly from $\eta = 0$ at $t = 0$ to $\eta = 0.1$ at $t = 50$ s. As seen from the figures, the aircraft response is stable and the autopilot tracks the pitch command, which is in agreement with the stability results presented in this section. Similar stable behavior was also noted, through simulations, for other velocities. It should be understood, however, that when strongly nonlinear phenomena take place, like saturation of the control surfaces or when the aircraft response enters the nonlinear aerodynamic region near stall, this analysis is no longer valid and cannot accurately predict the overall behavior of the aircraft.

IV. Envelope Protection Under Icing Conditions

The flight envelope of the aircraft changes under icing because the performance of the aircraft changes as a function of the icing severity.[1] This means that the aircraft envelope limits are now also a function of the icing parameter. Hence, conventional EP schemes, which use predetermined limits on parameters such as angle-of-attack, bank angle, and so forth, are no longer effective in icing conditions. This means that it is essential to introduce the concept of the iced-aircraft envelope, where the limits on the envelope have to be determined in real time, depending on the weather conditions,

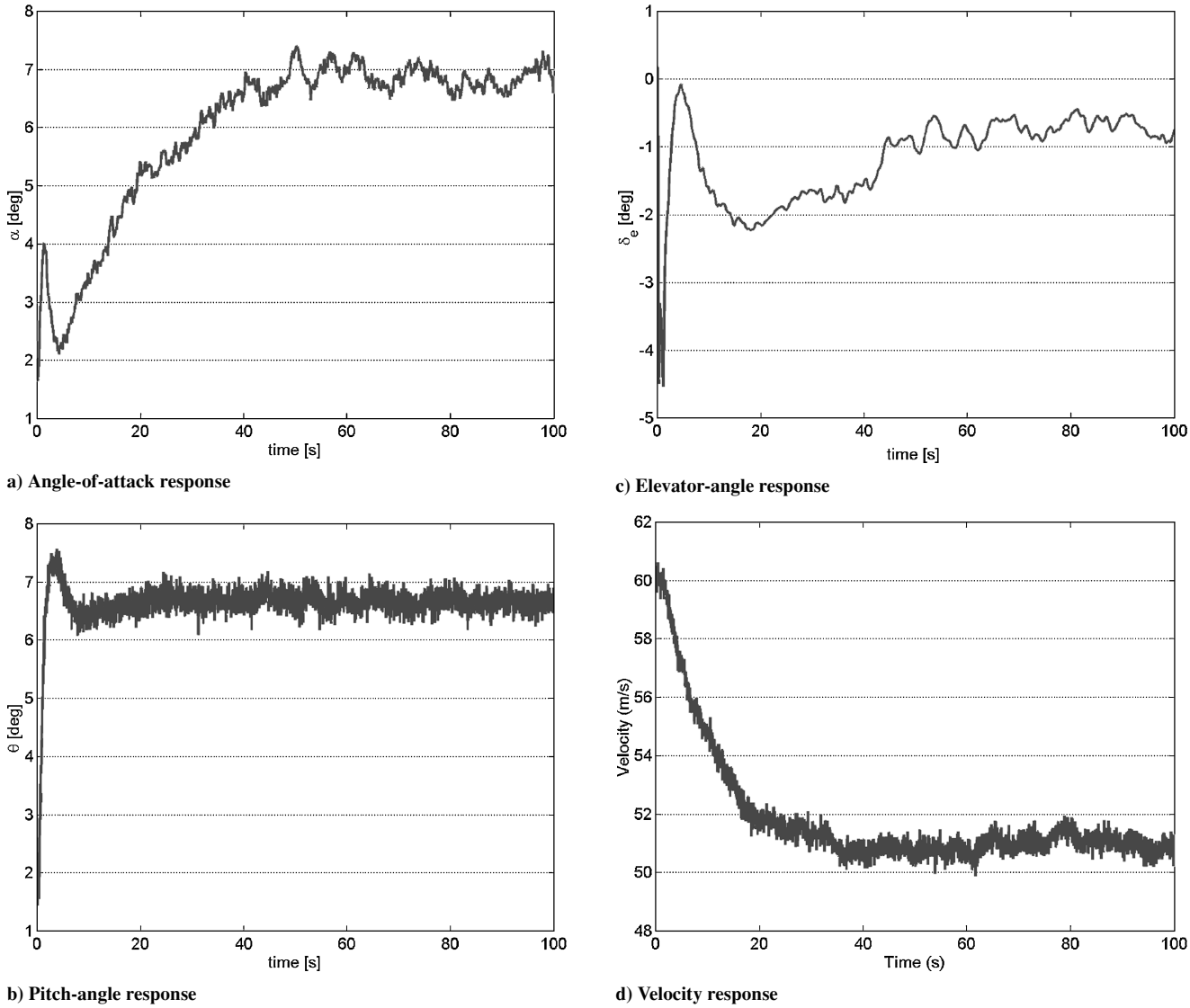

a) Angle-of-attack response

c) Elevator-angle response

b) Pitch-angle response

d) Velocity response

Fig. 3 Response of the PAH autopilot to a pitch-up maneuver of 5 deg at a velocity of 60 m/s with ice building up linearly from $\eta = 0$ at $t = 0$ to $\eta = \eta_{\max} = 0.1$ at $t = 50$ s.

and enforced dynamically to ensure flight safety. The aim of this section is to present the concept of an icing flight envelope and present an EP scheme that equips the autopilot with the ability to impose icing limits on itself and ensure it operates inside the icing flight envelope.

For an EP scheme to be effective, it should have a predictive capability so that it provides sufficient time to modify the input to the system and avoid envelope violation. Horn et al.[15,16] developed such a system for flight envelope cueing of tilt-rotor aircraft using parameter prediction algorithms based on available sensor data and control surface deflections. The system utilizes the functional dependence of the equations of motion and the envelope limits on the aircraft state. The method uses neural networks to estimate the so-called dynamic trim, which forms the basis of the protection algorithm.

In this paper we present a similar-in-spirit, prediction-based approach where the focus is placed on the fact that the aircraft dynamics and envelope change in time as a function of the icing level, from clean to iced.

A. Icing Envelope and Problem Formulation

In this paper, the issue of how to limit the reference pitch input command that is being issued to the system, so that the aircraft angle-of-attack response stays within stall angle limit, is addressed. To account for the change in the aircraft dynamics as a result of icing, the equations of motion include the icing parameter η as described in Ref. 1. Using the definitions of the state, the control, and icing parameter, the closed-loop equations of motion of the aircraft with PAH autopilot on can be written as

$$\dot{\boldsymbol{x}} = g(\boldsymbol{x}, \theta_{\text{ref}}, \eta) \tag{21}$$

where $\boldsymbol{x}$ is the state vector of the closed-loop PAH model. To complete the formulation, the flight envelope is expressed through the envelope parameter vector $\boldsymbol{y}_p$. The envelope parameter vector $\boldsymbol{y}_p$ consists of the critical parameters that need to be constrained within the safe flight envelope. The envelope parameter vector is defined as a function of the available state, the control, and icing parameter. The limits of the envelope parameter vector, that is, the maximum and minimum allowable values of the critical parameters at the given icing condition, are defined as functions of the icing parameter:

$$\boldsymbol{y}_p = \boldsymbol{y}_p(\boldsymbol{x}, \theta_{\text{ref}}, \eta) \tag{22}$$

$$\boldsymbol{y}_{\text{plim}} = \boldsymbol{y}_{\text{plim}}(\eta) \tag{23}$$

Thus, the EP problem considered is to provide a method to constrain the reference input θ_{ref} at each time instant to ensure envelope constraints:

$$\boldsymbol{y}^{l}_{\text{plim}} \leq \boldsymbol{y}_p \leq \boldsymbol{y}^{u}_{\text{plim}} \tag{24}$$

where $\boldsymbol{y}^{l}_{\text{plim}}$ and $\boldsymbol{y}^{u}_{\text{plim}}$ are the lower and upper limits respectively, on the critical parameter vector given by Eq. (23). This equation forms the core of the icing envelope because it describes the dependence of envelope limits on the icing parameter.

B. Critical Parameter and Its Limit Boundary

From a review of icing incidents and accidents it was found that an aircraft needed protection from wing stall, horizontal tail stall, roll upset, and loss of longitudinal and lateral control under icing conditions. For example, the ATR 72 accident of 1994 near Roselawn, Indiana was caused by roll upset, which resulted from the loss of roll control above a specific, but low, angle of attack.[17] A complete EP scheme needs to be developed that will provide protection from all the phenomena mentioned earlier. However, in this Paper, only the development of a system for the prevention of wing stall is addressed. To prevent stall, the aircraft angle of attack must be maintained at a value lower than the stall angle limit. Hence, the critical parameter vector is chosen to be the angle of attack, that is,

$$\boldsymbol{y}_p = \alpha \tag{25}$$

Having identified the critical parameter, it was necessary to define its boundaries as a function of data expected to be available for a SIS-equipped aircraft. To develop this capability, data spanning the entire envelope for different icing conditions were needed. However, because at this time only very limited data was available on iced aircraft limits from icing tests, a very basic method was developed to calculate the limits of the angle of attack using data obtained from wind-tunnel tests performed at the University of Illinois. The analysis was intended to identify trends in the performance degradation of an airfoil caused by simulated ice shapes. The idea was to develop the capability to determine the stall limits based on data available at low angle of attack. The most promising trend (linear) was found in the comparison of ΔC_L at constant angle of attack with iced airfoil $C_{L\max}$ data, where ΔC_L was the difference between the lift generated by an airfoil with simulated ice and the clean airfoil at the specified angle of attack.[11] Assuming a linear relation between stall angle of attack and the $C_{L\max}$, it was possible to define the limit value of the angle of attack as[11,18]

$$\alpha_{\text{stall}} = f(\Delta C_L) \tag{26}$$

where ΔC_L can be seen as a function of η.

C. Envelope Limiting Using Steady-State Estimation

An EP system built into an autopilot should be able to perform two functions: limit detection and limit avoidance. The system must detect the encroachment of an envelope limit, and then it must take measures to prevent the violation of the limit. Because there is a time lag between the reference input and the closed-loop response, a limit avoidance cueing system, based on instantaneous data, may allow inputs that will take the response of the aircraft beyond the allowable limits and, hence, it would not be a reliable EP system. Thus, it is necessary to have a prediction lead time; that is, it is desirable that the limit-detection algorithm estimate future values of a limited parameter in order to provide sufficient time margin for the autopilot system to react to it. Hence, given the icing parameter value, the EP system should be able to calculate the envelope limits and, based on those limits, identify the reference inputs to the autopilot beyond which the maximum response of the critical parameter will cross the limit in the future. Then it should constrain the θ_{ref} inputs within these values.

To check whether a particular input leads to exceeding the envelope limits, one has to run forward in time using Eq. (21) along with Eqs. (22) and (23) and check if Eq. (24) is satisfied. This constitutes, in principle, the natural basis of EP; that is, one can (on the fly) run forward using Eq. (22) assuming θ_{ref} is kept constant at its current value and check if angle-of-attack limits will be violated. If so, one can accordingly reduce θ_{ref} to a value that keeps the aircraft in the envelope.

A simple practical approach of doing predictions based on steady-state behavior is chosen. This has the advantage of requiring minimal online calculations; that is, we do not have to run Eq. (22) forward in time as it is basically done in Ref. 15. It is also based on the fact that with the PID controller used for the PAH autopilot, the angle-of-attack response for step inputs achieves the maximum at steady state at all flight conditions. The idea is to obtain limits on the reference pitch-angle values that are the input to the PAH autopilot so that the steady-state angle-of-attack response stays less than the stall angle. The effective prediction lead time that is achieved is the settling time of the step response. It should be noted that no claim on the convergence of this scheme is made and no theoretical proof of its successful operation is provided. Table 4 shows some limit values obtained using the steady-state analysis for the clean case for which the stall angle is 17.5 deg. Table 5 shows the limit values for the fully iced case with $\eta = 0.06$ for which the stall angle is 11.4 deg at a height of 2300 m.

D. Envelope Protection Module Based on Steady-State Analysis

Figure 4 shows the schematic of the autopilot system equipped with the EP scheme. It is assumed throughout the development that the icing-severity parameter η is estimated sufficiently accurately by some online icing characterization function. Such a

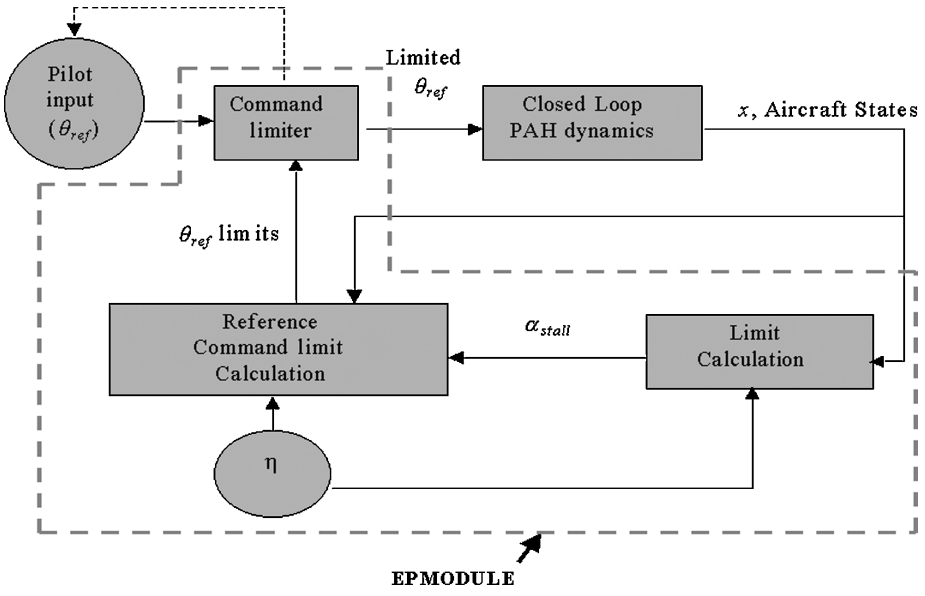

Fig. 4 Envisioned envelope protection system for the PAH autopilot.

Table 4 Maximum θ_{ref} allowed from steady-state analysis at different velocities for the clean case

Velocity, m/s	Maximum θ_{ref}, deg
60	9.5
65	10.9
70	12.7

Table 5 Maximum θ_{ref} allowed from steady-state analysis at different velocities for the iced case with $\eta = 0.06$

Velocity, m/s	Maximum θ_{ref}, deg
60	6.9
65	9
70	11.1

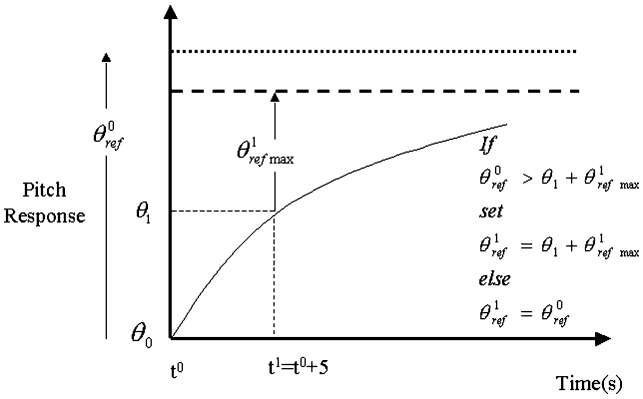

Fig. 5 Input command limiting scheme for envelope protection.

function is indeed feasible.[9,19] The EP module works in the following steps:

1) It obtains the angle-of-attack limit using the information on the currently available value of the icing parameter η.

2) It calculates the limit on θ_{ref} by using this limit on the angle of attack.

3) It then reduces the θ_{ref} input from the pilot, if required, to ensure it is inside the limit obtained in step 2 and sends a warning to the pilot.

The determination of limits on the reference pitch command is based on offline data collected for different flying conditions. A series of reference pitch commands are issued for several flying conditions, and different levels of icing and the steady-state values of the angle of attack for all situations are recorded in a variable along with the reference pitch commands, the trim velocity, and the ice parameter value to which they correspond. This can be done in simulation or looking at the dc gain of the transfer function from reference input to angle of attack for various η levels. The differences appeared to be small (at least when linear aerodynamic models with nonlinear equations of motion are considered). Then the steady-state angle-of-attack response at a given flying velocity, and ice parameter η to a reference pitch command, can be obtained from the data by using three-dimensional interpolation. At any time instance, a quick iteration finds out an estimate of the $\theta_{\text{ref max}}$ that is the maximum reference pitch input for which the angle-of-attack response just manages to stay within the stall limit at the current flying condition.

With this function at hand, the mechanism for EP works as follows: at any checking instance, the sum of $\theta_{\text{ref max}}$ and the current θ value is compared with the θ_{ref} issued at the previous checking instance; if the latter is greater than the former then it is reduced to equal the former. This check is done every 5 s. The procedure is depicted in Fig. 5. As shown in Fig. 5, every 5 s the EP module interpolates between data to obtain $\theta_{\text{ref max}}$ at the current flying conditions, using the current velocity and η value. It then checks whether $\theta_{\text{ref}} > \theta_1 + \theta_{\text{ref max}}$. If that is the case, then it sets $\theta_{\text{ref}} = \theta_1 + \theta_{\text{ref max}}$. If not, it leaves θ_{ref} unaltered. This function is incorporated into the autopilot part of the aircraft, where it checks for the reference pitch command every 5 s and modifies it if it is greater than the allowable reference pitch at that particular flying condition. Work is under way to incorporate the aforementioned EP module into the IEFS.[3]

E. Simulation Results

Two different situations are considered here: one where aerodynamics are linear and another where they are nonlinear. In both cases the overall model contained the nonlinear kinematics and dynamics. The first case was considered to test the command-limiting EP module and verify its effectiveness in protecting angle-of-attack excursions beyond stall. By employing a much more realistic aerodynamics model, the case with nonlinear aerodynamics, it was examined how dangerous the behavior can be if the EP is off. We mention here that all the SIMULINK simulations include the effects of the discretization of the controller and the EP scheme. These functions were running at 10 Hz. The simulations do not change even if the sampling hold elements run at substantially slower rates. Thus, from the hardware point of view, they are trustworthy.

1. Linear Aerodynamics Case

Two different scenarios are discussed in this subsection and the successful operation of the EP module is demonstrated.

1) The aircraft is initially trimmed at $V = 60$ m/s at a height of 2300 m with icing level of $\eta = 0.06$; that is, the aircraft is initially trimmed with iced condition and the icing level stays the same throughout the maneuver. The stall limit at this icing level is 11.4 deg. A pitch-up command of 7.6 deg is issued. Figure 6a shows the angle-of-attack response comparison for the case with the EP module off against the one with the EP module on. Clearly, for the case when the EP module is kept on, the angle-of-attack response does not violate the stall limit. This happens because the EP module manages to detect that the issued pitch-up command is greater than the maximum allowable value at this flying condition and cuts it down, as shown in Fig. 6c. The corresponding pitch response comparison is shown in Fig. 6b. Corresponding altitude, elevator, and velocity responses are shown in Figs. 6d, 6e, and 6f, respectively.

2) The aircraft is initially trimmed at a height of 2300 m and a velocity of 60 m/s under clean conditions. A pitch-up command of 7.6 deg is issued, and ice starts to build and grows from $\eta = 0$ at $t = 0$ to $\eta = 0.06$ at $t = 50$ s. As seen from Fig. 7a, the angle-of-attack response in the case where the EP scheme is not operational crosses the stall angle limit. Note that the limit is dynamic because of the change in the icing severity. The angle-of-attack stall limits starts from 17.6 deg under clean conditions and falls to 11.4 deg by 50 s, when the icing level reaches $\eta = 0.06$. In comparison, the EP scheme manages to sense the approaching α_{stall} dynamic limit and cuts down the reference pitch value as shown in Fig.7c to avoid the stall limit violation well in advance. Figs. 7e, 7f, and 7d show the corresponding elevator, velocity, and altitude responses, respectively.

In both of these scenarios, the response of the aircraft above the stall limit, when the EP module is off, is not realistic. That is, this "benign" behavior of the aircraft in stall is solely due to the linear aerodynamics model assumed, which really does not capture the poststall iced behavior described in Ref. 18. In that sense, these figures should be taken as a demonstration of successful angle-of-attack limiting when the EP module is on. A more realistic picture is given in what follows, where a poststall nonlinear icing aerodynamics model is used.[18]

2. Nonlinear Aerodynamics Case

Two cases are considered:

1) The aircraft is initially trimmed at a height of 2300 m and a velocity of 60 m/s under icing conditions with $\eta = 0.06$. A pitch-up command of 7.6 deg is issued. As seen from Fig. 8a, in the case where the EP scheme is not operational, the angle of attack crosses the stall angle limit, and the aircraft stalls with the altitude falling

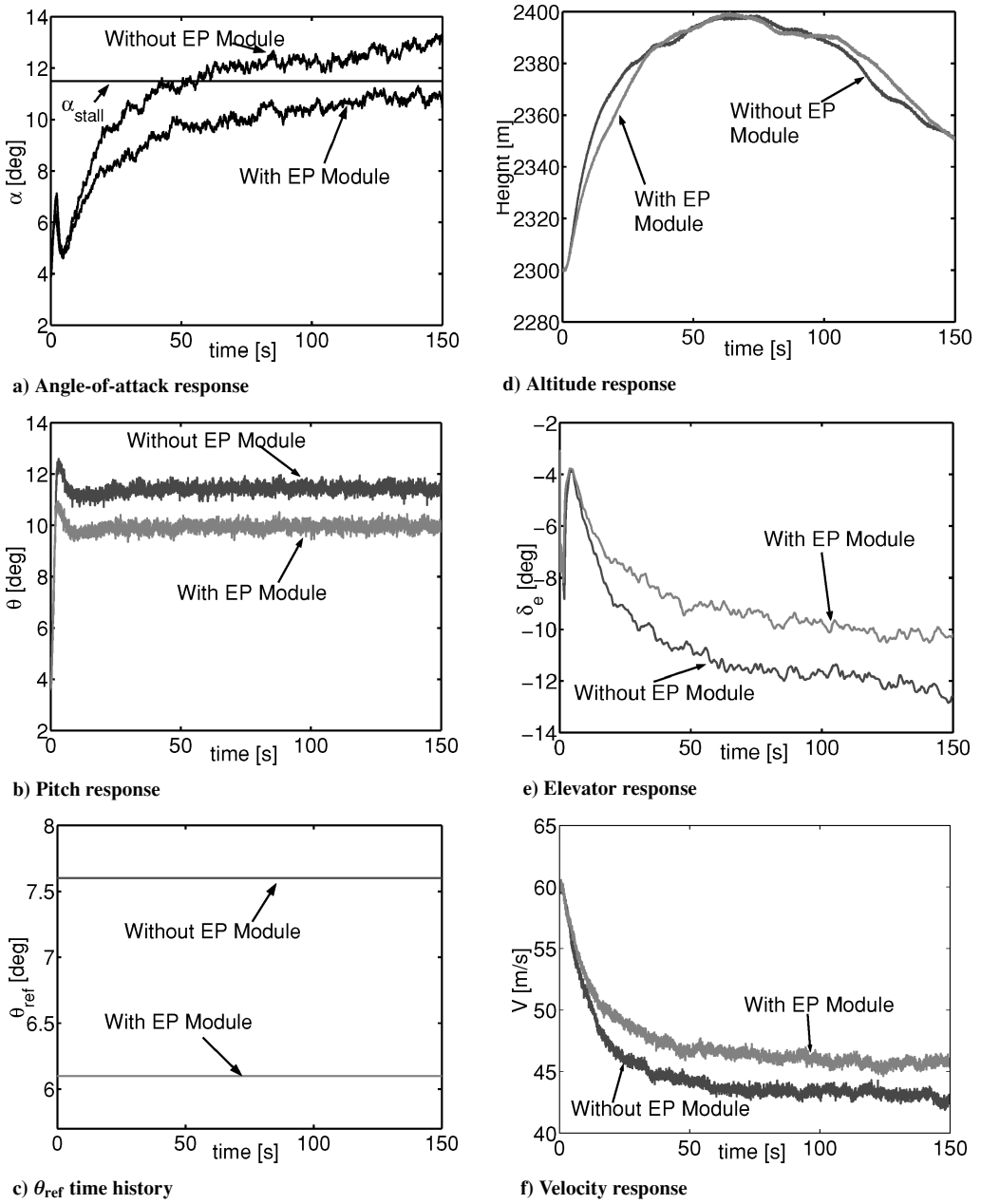

Fig. 6 Case 1: Different responses.

as shown in Fig. 8d. The stall limit is at around 11.4 deg at this icing level. In comparison, the EP scheme manages to sense the approaching α_{stall} limit and cuts down the reference pitch value as shown in Fig. 8c to avoid the stall limit, thus avoiding undesirable behavior.

2) The aircraft is initially trimmed under clean conditions at a height of 2300 m and a velocity of 60 m/s. A pitch-up command of 7.6 deg is issued. Ice starts to build from $\eta = 0$ at $t = 0$ to $\eta = 0.06$ at $t = 50$ s. As seen from Fig. 9a, the angle-of-attack response, in the case where the EP scheme is not operational, stalls after some time. The stall is also seen from Fig. 9d, where the height of the aircraft falls in the case where the EP module is not incorporated, indicating that it is dangerous to operate the autopilot under icing without the EP module. In comparison, the EP scheme manages to sense the approaching α_{stall} dynamic limit and cuts down the reference pitch value as shown in Fig. 9c to avoid the stall limit. Note that the stall limit is dynamic because of the varying icing level over time.

Many other simulations were run with nonlinear aerodynamics and it was seen that the EP module performed well to keep the aircraft response inside the iced envelope and maintain safe operation of the autopilot.

F. Discussion and an Alternative Approach

The previously mentioned EP scheme bases its predictions on steady-state offline data. The regular checking of the input command provides online adjustments that have proven in simulation to work effectively. An alternative approach, which is based on a worst-case scenario, is presented in what follows. It captures the relation between size of input and peak transients, assuming a worst-case input, and it can therefore provide a potential guide to EP. To this end, consider the form of the linearized closed-loop system,

$$\dot{x} = Ax + Bw, \qquad z = Cx + Dw \tag{27}$$

where z is an output vector that includes the critical parameters of the system we would like to limit, and w represents an exogenous input. For the purposes of EP, we choose w as the pitch reference input θ_{ref} and z is chosen as:

$$z = \begin{bmatrix} \alpha/\alpha_{\max} \\ \delta_e \big/ \delta_e^{\max} \end{bmatrix} \tag{28}$$

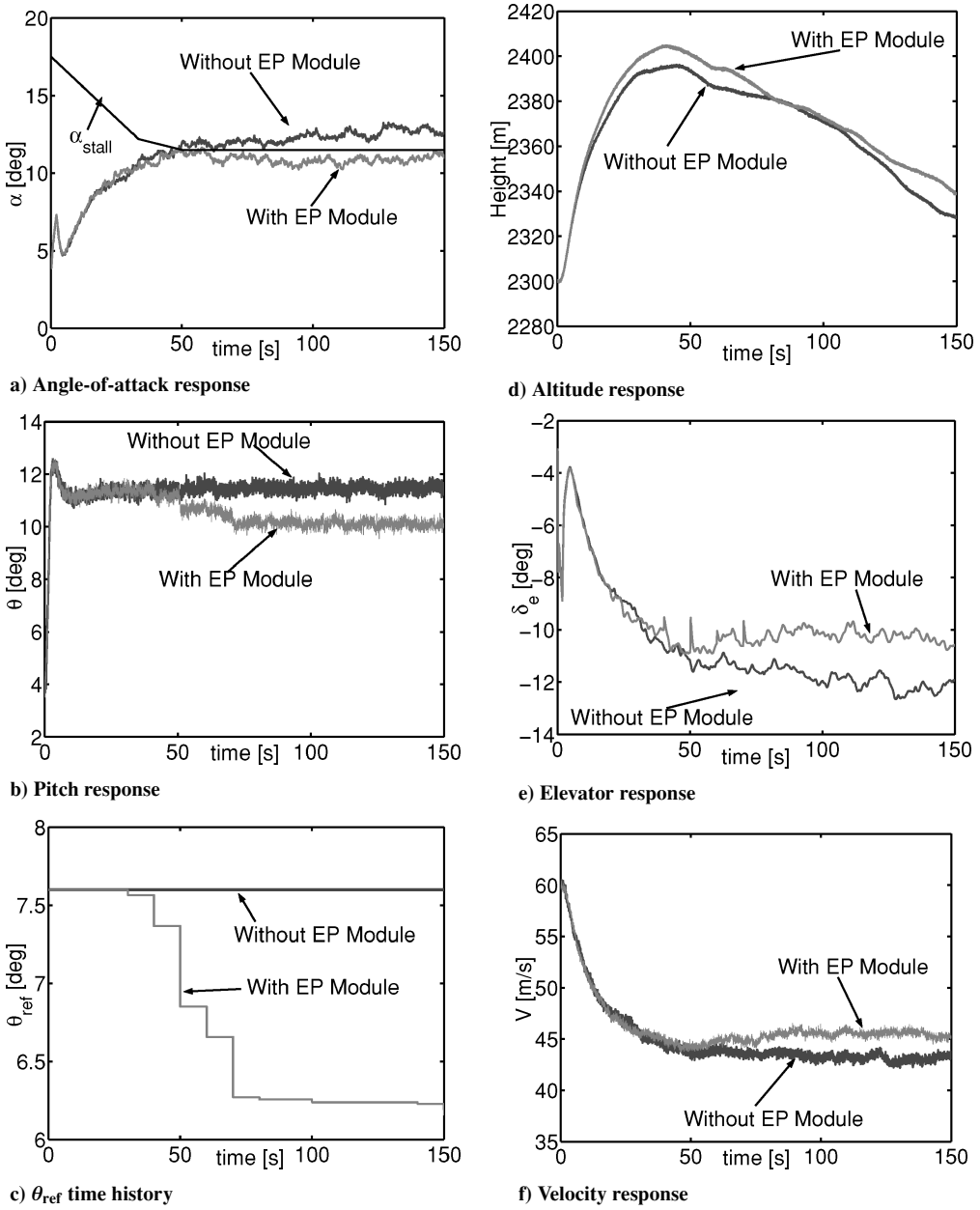

Fig. 7 Case 2: Different responses.

where $\alpha_{\max}$ is the maximum angle-of-attack value at the current icing level, and $\delta_e^{\max}$ is the maximum elevator deflection. Note that we included the deflection δ_e to capture elevator deflection limits. In the previously described EP scheme this was not an issue, because the steady-state angle-of-attack response will always dominate the steady-state elevator deflection. That is, stall limits will be reached without elevator saturation at steady state. Using Eq. (10) and defining

$$C_1 = [0 \quad 1/\alpha_{\max} \quad 0 \quad 0 \quad 0 \quad 0 \quad 0 \quad 0]$$

Eq. (28) can be rewritten as

$$z = \begin{bmatrix} C_1 x \\ \dfrac{1}{\delta_e^{\max}}(C_{\text{elv}} x_3 + D_{\text{elv}} u_3) \end{bmatrix} \tag{29}$$

Defining $\bar{C}_{\text{elv}} = C_{\text{elv}}/\delta_e^{\max}$, $\bar{D}_{\text{elv}} = D_{\text{elv}}/\delta_e^{\max}$, and using the definition of u_3 from the previous section, the preceding equation can be written as

$$z = \begin{bmatrix} C_1 \\ \bar{C} \end{bmatrix} x + \begin{bmatrix} 0 \\ \bar{E} \end{bmatrix} x_{\text{ref}} \tag{30}$$

where

$$\bar{C} = [-\bar{D}_{\text{elv}}(K_\theta + K_q) \quad \bar{D}_{\text{elv}} \quad \bar{C}_{\text{elv}}], \qquad \bar{E} = \bar{D}_{\text{elv}} K_\theta$$

Equation (30) can be rewritten as

$$z = \begin{bmatrix} C_1 \\ \bar{C} \end{bmatrix} x + \begin{bmatrix} 0 \\ \bar{D}_{\text{elv}} k_\theta \end{bmatrix} \theta_{\text{ref}} \tag{31}$$

Define

$$\bar{B}_{\text{closed}} = \begin{bmatrix} B_{\text{ac}} D_{\text{elv}} k_\theta \\ -K_i k_\theta \\ B_{\text{elv}} k_\theta \end{bmatrix}$$

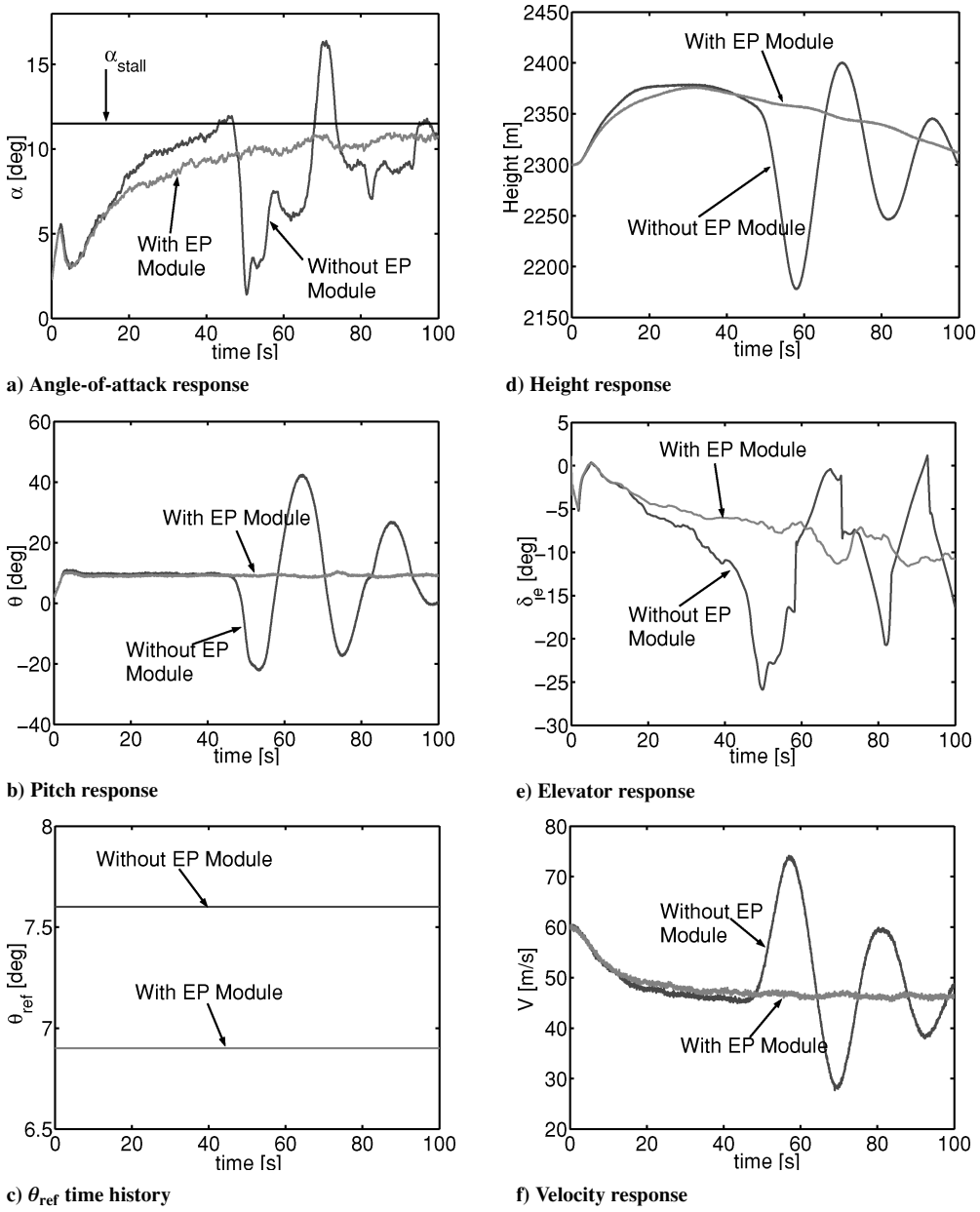

Fig. 8 Case 1 using nonlinear aerodynamics: Different responses.

The closed-loop PAH system can be rewritten as

$$\dot{x} = A_{\text{closed}} x + \bar{B}_{\text{closed}} \theta_{\text{ref}} \tag{32}$$

Now Eqs. (32) and (31) express closed-loop PAH autopilot in the form of Eq. (27) with

$$A = A_{\text{closed}}, \qquad B = \bar{B}_{\text{closed}}, \qquad C = \begin{bmatrix} C_1 \\ \bar{C} \end{bmatrix}$$

$$D = \begin{bmatrix} 0 \\ \bar{D}_{\text{elv}} k_\theta \end{bmatrix}, \qquad w = \theta_{\text{ref}} \tag{33}$$

Given this setup, we can look at the peak-to-peak gain of the closed loop given by the induced norm

$$\|T\|_{\infty,\infty} = \sup_{w \neq 0} \frac{\|z\|_\infty}{\|w\|_\infty} \tag{34}$$

where l_∞ is the space of signals $z : \Re_+ \to \Re^p$ of finite amplitude given by

$$\|z\|_\infty := \sup_{t \geq 0} \sqrt{z^T(t) z(t)}$$

Then the following gives a sufficient condition for $\|T\|_{\infty,\infty} < \gamma$.

Proposition 4.1: If there exists $K > 0$, $\lambda > 0$, and $\mu > 0$ such that

$$\begin{bmatrix} A^T K + K A + \lambda K & K B \\ B^T K & -\mu I \end{bmatrix} < 0$$

$$\begin{bmatrix} \lambda K & 0 & C^T \\ 0 & (\gamma - \mu) I & D^T \\ C & D & \gamma I \end{bmatrix} < 0 \tag{35}$$

the peak-to-peak norm of the system in Eq. (27) is smaller than γ.[§]

The implication is that to keep

$$|\alpha(t)| < \alpha_{\max}, \qquad |\delta_e(t)| < \delta_e^{\max} \tag{36}$$

[§]Taken from Scherer, C., and Weiland, S., "Linear Matrix Inequalities in Control," Course Notes from the Dutch Institute of Systems and Control.

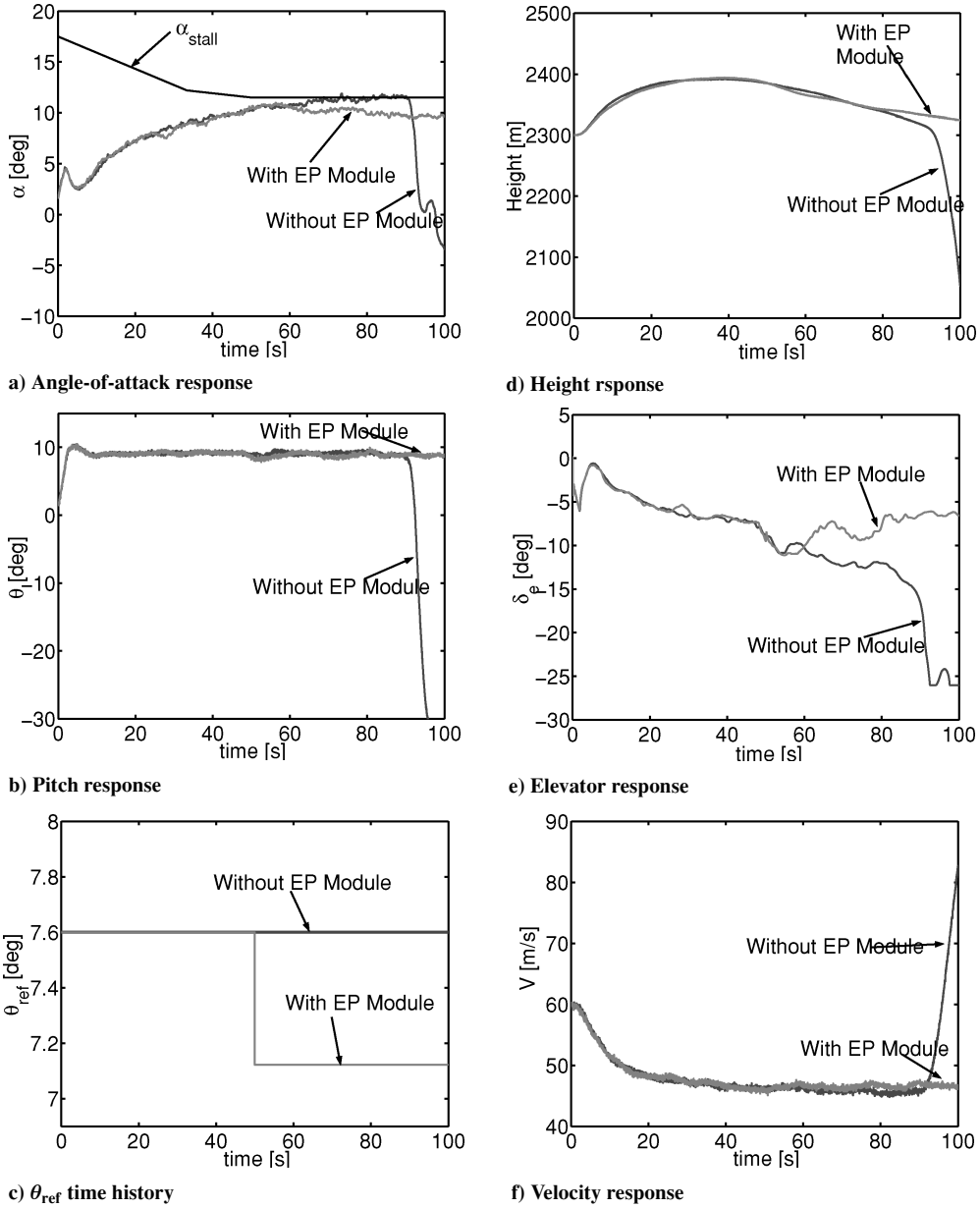

Fig. 9 Case 2 using nonlinear aerodynamics: Different responses.

for all time, it is enough to keep

$$\|z\|_\infty = \sup_{t\geq 0}\sqrt{z_1^2(t)+z_2^2(t)} = \sup_{t\geq 0}\sqrt{\left(\frac{\alpha(t)}{\alpha_{\max}}\right)^2+\left(\frac{\delta_e(t)}{\delta_e^{\max}}\right)^2} \leq 1 \tag{37}$$

The preceding inequality is guaranteed if $\|w\|_\infty < 1/\gamma$ or, equivalently, if

$$|\theta_{\text{ref}}(t)| < 1/\gamma \qquad \text{for all } t \tag{38}$$

This analysis suggests, therefore, a procedure to calculate an allowable range for θ_{ref} by calculating the minimum γ for which the LMI conditions in Eq. (35) are satisfied. Note that these LMIs should hold for all values of $\eta \in \triangle = [0, \eta_{\max}]$; that is, these conditions form an infinite set of constraints. However, the left-hand sides of these inequalities are affine functions of the parameter η, because the closed-loop state-space matrices are affinely dependent on η. Hence, the conditions in Eq. (35) need only be checked for $\eta \in \triangle_0 = \{0, \eta_{\max}\}$.[§] That corresponds to a finite set of LMIs in the variables K, λK, and μ. The problem now is to look for the minimum value of γ and solve for the LMIs in Eq. (35) evaluated at $\eta = 0$ and $\eta = \eta_{\max}$ and $K > 0$, $\lambda K > 0$, $\mu > 0$ in the variables K, λK, and μ. These obtained γ values give bounds on the closed-loop transfer-function-induced l_∞ norm for the linearized models at different flying conditions. This problem is solved using the LMI toolbox in MATLAB called the LMILAB for minimum values of γ that would satisfy the preceding system of LMIs. Table 6 shows some values obtained from the aforementioned techniques at different velocities.

Table 6 Minimum γ values obtained for $\eta_{\max} = 0.06$ at different velocities for the l_∞ norm analysis using LMI techniques

Velocity, m/s	γ
60	12.5
65	10
70	9.8

The procedure for obtaining γ limits on the induced l_∞ closed-loop norm is coded in MATLAB using LMILAB, and the

[§]Taken from Scherer, C., and Weiland, S., "Linear Matrix Inequalities in Control," Course Notes from the Dutch Institute of Systems and Control.

Table 7 Reference pitch limits obtained for PAH autopilot at different flying conditions for both the clean and iced conditions using LMI techniques

Clean case		Iced case ($\eta = 0.06$)	
Velocity, m/s	Maximum $\lvert\theta_{\text{ref}}\rvert$, deg	Velocity, m/s	Maximum $\lvert\theta_{\text{ref}}\rvert$, deg
60	6.0311	60	4.5837
65	7.5389	65	5.7296
70	5.8465	70	5.8465

corresponding limits on θ_{ref} obtained using Eq. (38) for an aircraft model linearized at different velocities are tabulated in Table 7. Note that values in this table are in degrees and are obtained by multiplying the corresponding γ values by $180/\pi$. From these tables it can be seen that this approach constrains the pilot input θ_{ref} more drastically than the previous method. This is expected, because this method assumes that a worst-case θ_{ref} is possible while, in fact, it may be an input that an ordinary pilot would never realize. This can provide some more robustness—to uncertainty in flying conditions, erroneous η estimates, as well as to unexpected pilot actions—at the expense of a more conservative icing envelope.

V. Conclusions

The effects of ice on the behavior of a typical PAH autopilot was investigated. The Twin Otter aircraft model was considered in this study as a representative type of commuter airplanes that appear to be the most sensitive to icing. A standard pitch attitude controller was chosen, with gains scheduled with respect to the aircraft velocity to provide good performance under clean conditions over the entire envelope. Using a time-varying model of the aircraft dynamics that depends affinely on an ice-severity parameter, a quadratic stability analysis was conducted to deduce that the (linearized) closed loop maintains stability under icing conditions. This fact was also confirmed through simulation results.

In addition to these analyses, a practical EP scheme was developed to keep the angle of attack within the (time-varying) iced envelope. In this approach, limits on the reference pitch values were obtained offline at different flying conditions such that the steady-state angle-of-attack response stayed within the stall limits. These data were then used to obtain a prediction lead time for online checking of the reference pitch inputs in order to avoid stall when the aircraft is in operation under the influence of ice accretion. The successful operation of this algorithm was demonstrated through simulations. An alternative, more conservative, LMI-based approach to obtain bounds on the allowable reference pitch commands was also presented. We mention at this point that we do not have an analytical proof of safety of the proposed EP scheme; it is only based on simulations. In that sense, it cannot be argued that it guarantees safety, nor can we argue that the allowed θ_{ref} will converge (assuming the pilot does not change his/her stick input). The situation is quite similar to gain scheduling where, typically, only through simulations can stability be demonstrated for the entire operational range.

This paper investigated only the behavior of the PAH autopilot under icing conditions and it therefore constitutes an initial and partial study on the effects of ice accretion on aircraft safety. Current research is under way to study such safety issues related to other autopilot modes of operation. Moreover, the PAH model of the autopilot used here has already been integrated into the IEFS being developed at the University of Illinois, and further work is under way to incorporate and test the EP scheme developed in this paper. In addition, initial flight testing[10] has been done and we plan to test these algorithms on a real platform.

The simulation results of this Paper have indicated that a simple EP scheme is good enough to avoid stall and no controller adaptation is necessary. However, it still remains an open question as to how well, if at all, an airplane can recover from a severe envelope violation. Control reconfiguration/adaptation has the potential to provide some answers to these types of questions and it is currently under investigation.

Acknowledgments

The work of the first and the second author was supported by NASA Grant NAG 3-125.

References

[1]Bragg, M. B., Hutchison, T., Merret, J., Oltman, R., and Pokhariyal, D., "Effect of Ice Accretion on Aircraft Flight Dynamics," AIAA Paper 2000-0360, Jan. 2000.

[2]Bragg, M. B., Basar, T., Perkins, W. R., Selig, M. S., Voulgaris, P. G., and Melody, J. W., "Smart Icing Systems for Aircraft Icing Safety," AIAA Paper 2002-0813, Jan. 2002.

[3]Sehgal, B., Deters, R., and Selig, M. S., "Icing Encounter Flight Simulator," AIAA Paper 2002-0817, Jan. 2002.

[4]Rauw, M., FDC 1.3—A SIMULINK Toolbox for Flight Dynamics and Control Analysis, 1998, available at http://www.mathworks.com/matlabcentral/fileexchange [cited October 2000].

[5]Pokhariyal, D., "Effect of Ice Accretion on Aircraft Performance and Control During Trimmed Flight," M.S. Thesis, Aeronautical and Astronautical Engineering Dept., Univ. of Illinois, Urbana, IL, 2000.

[6]Ratvasky, T., and Ranaudo, R., "Icing Effects on Aircraft Stability and Control Determined from Flight Data," AIAA Paper 93-0398, Jan. 1993.

[7]Dimock, G. A., Deters, R., and Selig, M. S., "Icing Scenarios with the Icing Encounter Flight Simulator," AIAA Paper 2003-0023, Jan. 2003.

[8]Roskam, J., *Airplane Flight Dynamics and Automatic Flight Controls*, 2nd ed., Roskam Aviation and Engineering Corp., Ottawa, Canada, 1982.

[9]Melody, J. W., Basar, T., Perkins, W. R., and Voulgaris, P. G., "Parameter Identification for Inflight Detection and Characterization of Aircraft Icing," *Control Engineering Practice*, Vol. 8, Sept. 2000, pp. 985–1001.

[10]Whalen, E., Lee, S., and Bragg, M. B., "Characterizing the Effect of Ice on Aircraft Performance and Control from Flight Data," AIAA Paper 2002-0816, Jan. 2002.

[11]Hossain, K. N., "Envleope Protection in Icing Encounters," M.S. Thesis, Aeronautical and Astronautical Engineering Dept., Univ. of Illinois, Urbana, IL, 2003.

[12]Mccormick, B. W., *Aerodynamics, Aeronautics and Flight Mechanics*, Wiley, New York, 1979, Chap. 9, p. 552.

[13]Boyd, S., El Ghaoui, L., Feron, E., and Balakrishnan, V., *Linear Matrix Inequalities in System and Control Theory*, Vol. 15, Studies in Applied Mathematics, Society for Industrial and Applied Mathematics, Philadelphia, 1994, pp. 61, 62, 66, 67.

[14]Gahinet, P., Nemirovski, A., Laub, A. J., and Chilali, M., LMI Control Toolbox: For Use with MATLAB, Mathworks Partner Series, Mathworks Inc., Natick, MA, 1995.

[15]Horn, J., Calise, A. C., and Prasad, J. V. R., "Development of Envelope Protection Systems for Rotorcraft," *Proceedings of the 55th Annual Forum American Helicopter Society*, American Helicopter Society, Alexandria, VA, 1999, pp. 2025–2036.

[16]Horn, J., Calise, A. C., Prasad, J. V. R., and O'Rourke, M., "Flight Envelope Cueing on a Tilt-Rotor Aircraft Using Neural Network Limit Prediction," *Proceedings of the 54th Annual Forum American Helicopter Society*, American Helicopter Society, Alexandria, VA, 1998, pp. 1093–1104.

[17]Board, N. T. S., "Aircraft Accident Report: Inflight Icing Encounter and Loss of Control Simmons Airlines, d.b.a American Eagle Flight 4184 Avions de Transport Regional (ATR) Model 72-2122, N401AM, Roselawn, Indiana, October 31, 1994," National Transportation Safety Board Rept. NTSB/AAR-96/01, PB96-910401, Vol. 1, July 1996.

[18]Hossain, K. N., Sharma, V., Bragg, M. B., and Voulgaris, P. G., "Envelope Protection and Control Adaptation in Icing Encounters," AIAA Paper 2003-0025, Jan. 2003.

[19]Melody, J., Pokhariyal, D., Merret, J., Basar, T., Perkins, W. R., and Bragg, M. B., "Sensor Integration for Inflight Icing Characterization Using Neural Networks," AIAA Paper 2001-0542, Jan. 2001.